

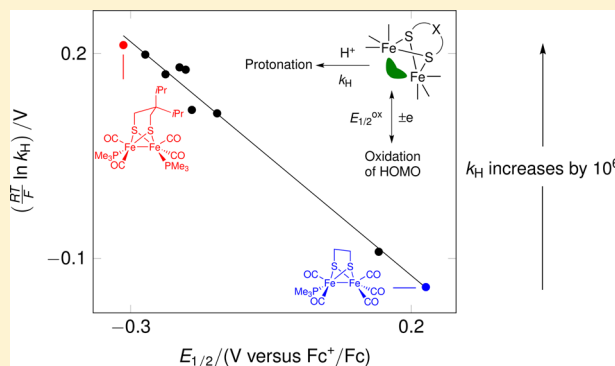
Electronic Control of the Protonation Rates of Fe–Fe Bonds

Aušra Jablonskytė, Lee R. Webster, Trevor R. Simmons, Joseph A. Wright, and Christopher J. Pickett*

Energy Materials Laboratory, School of Chemistry, University of East Anglia, Norwich Research Park, Norwich NR4 7TJ, United Kingdom

Supporting Information

ABSTRACT: Protonation at metal–metal bonds is of fundamental interest in the context of the function of the active sites of hydrogenases and nitrogenases. In diiron dithiolate complexes bearing carbonyl and electron-donating ligands, the metal–metal bond is the highest occupied molecular orbital (HOMO) with a “bent” geometry. Here we show that the experimentally measured rates of protonation (k_H) of this bond and the energy of the HOMO as measured by the oxidation potential of the complexes ($E_{1/2}^{\text{ox}}$) correlate in a linear free energy relationship: $\ln k_H = ((F(c - \beta E_{1/2}^{\text{ox}}))/(RT))$, where c is a constant and β is the dimensionless Brønsted coefficient. The value of β of 0.68 is indicative of a strong dependence upon energy of the HOMO: measured rates of protonation vary over 6 orders of magnitude for a change in $E_{1/2}^{\text{ox}}$ of ca. 0.55 V (ca. 11 orders of magnitude/V). This relationship allows prediction of protonation rates of systems that are either too fast to measure experimentally or that possess additional protonation sites. It is further suggested that the nature of the bridgehead in the dithiolate ligand can exert a stereoelectronic influence: bulky substituents destabilize the HOMO, thereby increasing the rate of protonation.



INTRODUCTION

The protonation of diiron dithiolate complexes such as those based on the $[\text{Fe}_2(\text{SCH}_2\text{XCH}_2\text{S})(\text{CO})_{(6-n)}\text{L}_n]$ assembly (X = alkyl, N -alkyl, NH , O , S , Se ; n = 0 to 4) to give bridging or terminal hydride products has received considerable attention over the past 10 years.^{1,2} This has been primarily driven by the need to understand the structure and function of the subsite of $[\text{FeFe}]$ -hydrogenase and provide knowledge for the design of artificial (electro)catalytic systems for hydrogen production/uptake.^{3,4} The generation of bridging hydrides at metal–metal bonded systems is of relevance to other metallosulfur enzyme active sites, for example, the FeMoco center of nitrogenase,⁵ the $[\text{NiFe}]$ -hydrogenase,^{1,2} CO dehydrogenase⁶ and also in establishing general mechanistic principles of protonation at metal centers.

Protonation of Fe(I)Fe(I) diiron dithiolate units can occur at the metal–metal bond to give bridging hydrides⁷ or at a single iron site to give a terminal hydride.^{8–11} In earlier work it was thought that a terminal hydride intermediate was on the pathway to the formation of the thermodynamically more stable bridging hydride.⁹ However, it was later shown that at low temperature bridging hydrides are formed more rapidly in certain electron-rich systems than are the terminal species.¹⁰ Furthermore, terminal hydrides have not been detected as intermediates in less basic systems, which give bridging hydrides under ambient conditions. While the natural system possesses CN^- coligands, herein we have examined diiron units with PMe_3 substituents.¹² This has the advantage in that alternative protonation on CN^- is avoided, but the electron-

donating properties are retained; notably, in the natural system the cyanide ligands are hydrogen bonded and do not present protonation sites.

In earlier studies we have shown that the rate of protonation of dithiolate systems is dependent on the nature of the X in the dithiolate ligand.^{13–15} For example, the complex $\text{Fe}_2(\text{odt})(\text{CO})_4(\text{PMe}_3)_2$ (odt = 2-oxapropane-1,3-dithiolate) is protonated at the metal–metal bond roughly 1 order of magnitude more slowly than $\text{Fe}_2(\text{pdt})(\text{CO})_4(\text{PMe}_3)_2$ (pdt = propane-1,3-dithiolate): in neither case was a terminal hydride detected. In this study we sought to unravel how the nature of the bridging dithiolate and the coligand(s) control the overall rate of protonation at $\{2\text{Fe}2\text{S}\}$ and $\{2\text{Fe}3\text{S}\}$ cores (containing two iron atoms and two or three sulfur atoms, respectively). We show that bulky bridgehead units, which are known to stabilize mixed valence Fe(I)Fe(II) cations,¹⁶ can also influence the rate of formation of $\text{Fe(II)}(\mu\text{-H})\text{Fe(II)}$ cations. Noting the earlier pioneering work of Norton and co-workers, which showed that protonation at metal centers can be slow,¹⁷ and studies by Henderson and co-workers on the protonation of Mo and W hydrides^{18,19} and on iron–sulfur clusters,²⁰ which leads to hydrogen evolution or substrate reduction, studies of the factors that control protonation rates at metal centers are relatively few.

Received: July 3, 2014

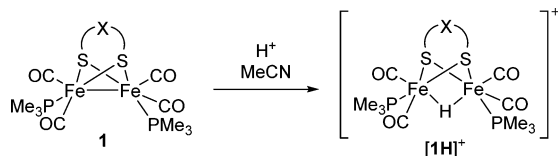
Published: August 12, 2014

RESULTS AND DISCUSSION

Synthesis. The compounds used in this study were synthesized by literature methods or by modification of these as described in the Supporting Information (SI). Among the new compounds reported are hexacarbonyl precursors with one or two isopropyl substituents on the dithiolate bridgehead, together with their PMe_3 derivatives, and related monomethyl species.

Kinetic Measurements. Stopped-flow (SF) methods have previously allowed examination and protonation rates for **1**(pdt), **1**(edt) and **1**(odt) (Scheme 1, edt = ethane-1,2-

Scheme 1. Protonation of $\text{Fe}_2(\text{xdt})(\text{CO})_4(\text{PMe}_3)_2^a$



^aThere is turnstile interchange of the CO and PMe_3 ligands at the metal centers.²³ General conditions: complex concentration 0.12–0.50 mM, acid ($\text{HBF}_4 \cdot \text{Et}_2\text{O}$) concentrations cover the range 5–250 mM, 21 °C, reaction under N_2 or Ar.

dithiolate), revealing significant variation in the primary protonation rate.^{13–15} However, the reasons underpinning this variation was not apparent; notably the closely similar $\tilde{\nu}(\text{CO})$ infrared data suggests minimal electronic influence by the bridgehead substituent X.^{16,21,22} To probe the relationship between structure and reactivity further we have studied a series of established and new diiron dithiolates of general formula $\text{Fe}_2(\text{xdt})(\text{CO})_{(6-n)}(\text{PMe}_3)_n$ ($n = 1$ or 2) and have determined protonation rates under directly comparable conditions.

The reaction of **1**(*i*Pr-pdt) (*i*Pr-pdt = 2-isopropylpropane-1,3-dithiolate) with $\text{HBF}_4 \cdot \text{Et}_2\text{O}$ in MeCN proceeds quantitatively to give the bridging hydride product $[\text{1H}(\text{iPr-pdt})]^+$. This species was isolated and fully characterized, and its structure was confirmed by X-ray crystallography (see SI for details). Figure 1 (left) shows a typical time-course for the protonation of **1**(*i*Pr-pdt) under pseudo-first-order conditions of acid, as measured at 348 nm in an SF UV–visible experiment. Over a range of concentrations of $\text{HBF}_4 \cdot \text{Et}_2\text{O}$ the decays each fit to single exponential curves from which the pseudo-first-order rate constants (k_{obs}) were estimated. Figure 1 (right) shows the plot of k_{obs} versus $[\text{HBF}_4 \cdot \text{Et}_2\text{O}]$ from which the second order rate

constant (k_{H}) for protonation was estimated to be $1190(40) \text{ M}^{-1} \text{ s}^{-1}$. Rate constants (k_{H}) for the compounds listed in Table 1 were similarly determined either by SF UV–visible or SF FT-IR techniques.

Our previous stopped-flow studies have established that rapid primary protonation in these systems is followed by isomerization on a slower time scale, on the order of tens of seconds to minutes depending on the bridge.^{13,14} In the current paper we focus on the primary protonation step: this is distinguished from the later isomerizations as only the first phase of reaction leads to a change in the UV spectrum and discernible change in the IR. At room temperature the dynamics of isomer interconversion of the *unprotonated* complexes is fast, whereas product interconversion is slow.²³

Inspection of Table 1 reveals the gross trends in protonation rates. First, for those complexes for which k_{H} can be directly determined, the rate constants span 6 orders of magnitude. Second, the more electron-donating PMe_3 groups installed at the dithiolate core, the faster is the protonation rate: protonation of the tetrakis(trimethylphosphine) complex **7** is immeasurably fast, while that for the hexacarbonyl **2** is not observed because $\text{HBF}_4 \cdot \text{Et}_2\text{O}$ is an insufficiently strong acid to protonate **2**.²⁴ We do not detect terminal hydride intermediates in any of the systems amenable to SF FT-IR study at 294 K.

For the five bis(trimethylphosphine) complexes **1** in which the bridgehead 2-substitution is varied on the propanedithiolate framework the reaction rate ranges increase by a factor of 5 on going from the unsubstituted pdt complex to the bis(isopropyl) substituted species. While this variation accords with the enhanced inductive resulting from the bridgehead dialkyl substituents on the diiron unit, the enhancement of rate for monoalkyl substitution is minimal (Table 1). Notably, FT-IR frequencies for the **1**(pdt, Me-pdt, *i*Pr-pdt) are essentially indistinguishable (Table 2), which is consistent with the closely similar rates.^{15,16,21,22}

The Nature of the Site of Protonation: The Energy of the HOMO. The site of protonation in all the complexes studied by SF FT-IR is the metal–metal bond. Photoelectron spectroscopy and DFT calculations have shown that in a typical $\text{Fe}_2\text{S}_2(\text{CO})_6$ unit the orbital character of the HOMO (highest occupied molecular orbital) corresponds closely to the classical “bent” Fe–Fe bond.^{25–27} Thus, the protonation of the metal–metal bond and the oxidation of diiron complexes engages the HOMO directly. If a reversible one-electron oxidation process in solution is considered, then the value of formal potential E^0 (close to $E_{1/2}$)²⁸ can be viewed as a relative measure of the

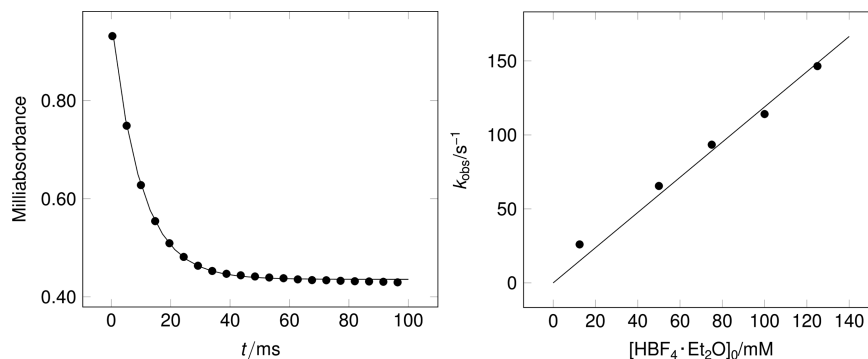
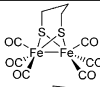
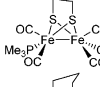
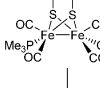
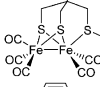
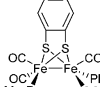
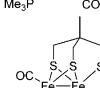
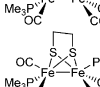
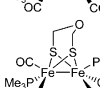
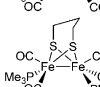
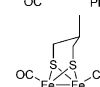
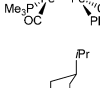
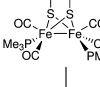
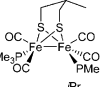
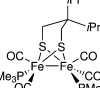


Figure 1. Left: Decay of UV signal at 348 nm over time on protonation of **1**(*i*Pr-pdt) (circles); pseudo-first-order fit (line); $[\text{1}(\text{iPr-pdt})]_0$ 0.13 mM, $[\text{HBF}_4 \cdot \text{Et}_2\text{O}]_0$ 125 mM. Right: Rates of protonation of **1**(*i*Pr-pdt) in MeCN as measured by UV over a range of acid concentrations. The linear fit for k_{obs} versus $[\text{HBF}_4 \cdot \text{Et}_2\text{O}]$ plot is that for a fixed zero intercept.

Table 1. Second Order Rate Constants for Protonation^a and Oxidation Potentials, $E_{1/2}^{\text{ox}}$, for Parent Complexes^b

Entry	Complex	Structure	$k_H/\text{M}^{-1} \text{s}^{-1}$	$E_{1/2}/\text{V}$ vs Fc^+/Fc
1	2(pdt)		no reaction	+0.65
2	3(edt)		0.0037(4) ^c	+0.23
3	3(pdt)		0.0284(18) ^c	+0.014
4	4		0.057(1) ^c	+0.23
5	5		9.3(3) ^c	-0.15
6	6		47(2)	-0.16
7	1(edt)		83.7(11) ¹⁴	-0.15
8	1(odt)		102(2) ¹⁵	-0.19
9	1(pdt)		797(16) ¹³	-0.24
10	1(Me-pdt)		1040(30)	-0.20
11	1(iPr-pdt)		1190(40)	-0.21
12	1(Me ₂ -pdt)		2480(40)	-0.27
13	1(iPr ₂ -pdt)		4300(150)	-0.31
14	7(pdt)		$>8 \times 10^5$	-1.12

^aProtonation carried out using $\text{HBF}_4 \cdot \text{Et}_2\text{O}$ in MeCN at 21 °C; protonation rates determined by stopped-flow UV unless otherwise noted.^bMeasured at vitreous carbon electrode in 0.1 M $[\text{Bu}_4\text{N}][\text{BF}_4]$ -MeCN, under argon. ^cProtonation rates determined by stopped-flow IR.

Table 2. Comparison IR Stretching Frequencies (MeCN) for 1(xdt)

Entry	Bridge	$\tilde{\nu}/\text{cm}^{-1}$
1	edt	1982, 1944, 1908, 1898 sh ¹⁴
2	odt	1984, 1947, 1913, 1898 sh ¹⁵
3	pdt	1980, 1943, 1898 ¹³
4	Me-pdt	1980, 1943, 1899
5	iPr-pdt	1980, 1943, 1899
6	Me ₂ -pdt	1980, 1939, 1900
7	iPr ₂ -pdt	1978, 1971, 1939, 1899

energy of the HOMO for a series of complexes where solvation energy differences between oxidized and reduced forms are very similar or vary systematically.²⁹

Cyclic voltammetry (CV) of the complexes was carried out under an argon atmosphere in 0.1 M $[\text{Bu}_4\text{N}][\text{BF}_4]$ -MeCN solutions, and revealed a clear variation in $E_{1/2}$ values (Table 1). The voltammograms also demonstrate that the presence of sterically demanding groups results in a much more stable product: oxidation of 1(iPr₂-pdt) and 1(Me₂-pdt) is fully reversibly at low scan rates (50 mV s⁻¹), whereas in all other cases only partially reversible waves were observed (see SI). $E_{1/2}^{\text{ox}}$ values for the monophosphine complexes are significantly

more positive than those for the related disubstituted analogues. The extent to which the HOMO is raised in energy by increasing the degree of substitution of PMe_3 ligands at the diiron core is illustrated in Figure 2. The linear relationship

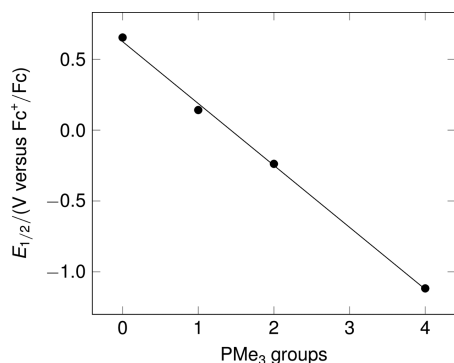


Figure 2. Correlation of oxidation potential with degree of phosphine substitution in the series $\text{Fe}_2(\text{pdt})(\text{CO})_{(6-n)}(\text{PMe}_3)_n$, $n = 0, 1, 2, 4$. Oxidation potentials were recorded at a vitreous carbon electrode in 0.1 M $[\text{Bu}_4\text{N}][\text{BF}_4]\text{-MeCN}$ and are reported relative to a Fc^+/Fc internal standard.

conforms to an additivity of substituent influence previously recognized in progressive substitution of CO in mononuclear complexes by donor ligands.³⁰ It is perhaps surprising that the single (asymmetric) substitution fits with this correlation; this presumably reflects extensive delocalization of electron density in the $\{2\text{Fe}2\text{S}\}$ core.

There is a linear correlation ($r^2 = 0.985$) between the oxidation potential of the complexes and the activation energy of the protonation reaction at 294 K, as is evident from the plot of $(RT/F) \ln k_{\text{H}}$ versus $E_{1/2}^{\text{ox}}$ (Figure 3). Taking the value of

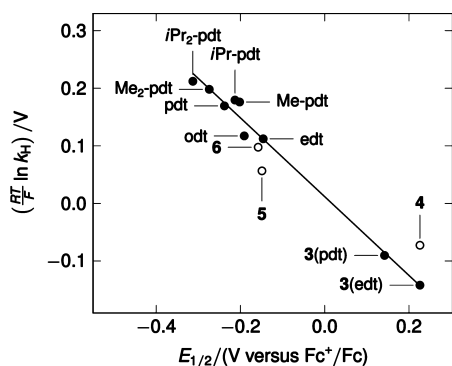


Figure 3. Correlation of rate of protonation with oxidation potential for $\{2\text{Fe}2\text{S}\}$ and $\{2\text{Fe}3\text{S}\}$ systems. Where not specified, substrates are of general structure 1. The line shows the best-fit for the filled circles: substrates of general structure $\text{Fe}_2(\text{xdt})(\text{CO})_{(6-n)}(\text{PMe}_3)_n$, xdt = alkyl dithiolate, $n = 1, 2$. Oxidation potentials were recorded at a vitreous carbon electrode in 0.1 M $[\text{Bu}_4\text{N}][\text{BF}_4]\text{-MeCN}$ and are reported relative to a Fc^+/Fc internal standard. Protonation rates were measured by stopped-flow IR [3(edt), 3(pdt), 4, 5] or UV (all others).

the gas constant $R = 8.314 \text{ J mol}^{-1} \text{ K}^{-1}$ and that of the Faraday constant $F = 9.649 \times 10^4 \text{ J mol}^{-1} \text{ V}^{-1}$, there is parity in the units of the x - and y -axes, i.e., volts. The dimensionless slope is -0.68 , which is strongly indicative that the ground-state energy of the HOMO has a determining influence on the activation energy. Explicitly, for the series of dialkyl dithiolate PMe_3 complexes, an increase in the energy of the HOMO by 100 kJ

mol^{-1} lowers the activation energy for protonation by 68 kJ mol^{-1} at 294 K.³¹

Whereas the dominant correlation of $\ln k_{\text{H}}$ against $E_{1/2}^{\text{ox}}$ is readily understood in terms of the donicity of the substituent groups at the diiron core, as discussed above, the infrared data for the bridgehead alkyl substituted compounds would suggest that there is at first sight a minimal electronic effect of these groups on the core. In accord with this, for the CH_2 , CHMe and $\text{CH}(\text{iPr})$ bridgeheads [1(pdt), 1(Me-pdt) and 1($i\text{Pr}$ -pdt), respectively], the measured $E_{1/2}^{\text{ox}}$ values and infrared frequencies are closely similar, as are the magnitudes of k_{H} . However, the dialkyl bridgehead complexes 1($\text{Me}_2\text{-pdt}$) and 1($i\text{Pr}_2\text{-pdt}$) show enhanced rates and more negative $E_{1/2}^{\text{ox}}$ values than might be expected from the FT-IR data (Table 2). Changes in $\tilde{\nu}(\text{CO})$ have previously been correlated with $E_{1/2}^{\text{ox}}$ in mononuclear monocarbonyl species, where $\Delta\tilde{\nu}(\text{CO})/\Delta E_{1/2}^{\text{ox}}$ is of the order of $100 \text{ cm}^{-1}/\text{V}$.³² Using data reported by Ott and co-workers for the protonated and unprotonated forms of $\text{Fe}_2(\text{Bn-adt})(\text{CO})_4(\text{PMe})_2$ ($\text{Bn-adt} = N\text{-benzyl-2-azapropane-dithiolate}$, $\text{Bn} = \text{benzyl}$),³³ $\Delta\tilde{\nu}_{\text{ave}}(\text{CO})/\Delta E_{1/2}^{\text{ox}}$ may be estimated at ca. $60 \text{ cm}^{-1}/\text{V}$ for diiron dithiolate systems bearing four CO groups. On this basis we might expect $\Delta\tilde{\nu}_{\text{ave}}(\text{CO})$ of ca. 5 cm^{-1} between 1(pdt) and 1($i\text{Pr}_2\text{-pdt}$) ($\Delta E_{1/2}^{\text{ox}} = 75 \text{ mV}$), which rather emphasizes the poor sensitivity of changes in IR frequencies and judging the effect of bridgehead structural change vis à vis $\Delta E_{1/2}^{\text{ox}}$.³⁴

It is therefore rather more pertinent to consider the substantial change in $E_{1/2}^{\text{ox}}$ between the monoalkylated and dialkylated bridgehead against the minimal change observed between the unsubstituted and monoalkylated forms and the possibility of a stereoelectronic effect. The solid-state structures of the complexes 1($i\text{Pr}$ -pdt) and 1($i\text{Pr}_2\text{-pdt}$) are shown in Figure 4, from which it is clear that the dialkyl bridgehead complex has a semibridging CO group, whereas the monoalkyl bridgehead complex has an essentially all-terminal arrangement of CO ligands. The former parallels the solid state for a diethyl bridgehead complex by Darensbourg and co-workers, which also displays a semibridging CO group.^{22,35} Infrared studies show that in MeCN solution there is not a detectable population of the semibridged carbonyl form. In addition ^{31}P NMR spectra at room temperature for unsubstituted, mono- and dialkyl-substituted show single ^{31}P resonances. This apparently contradictory spectroscopic, kinetic and $E_{1/2}$ data can be reconciled as follows.

Density functional theory (DFT) calculations were undertaken for 1(Me-pdt) and 1($\text{Me}_2\text{-pdt}$). For 1(Me-pdt) minimization from either an all-terminal or semibridging initial geometry results in identical minima in which all of the carbonyl groups are terminal. In contrast, minimizations of 1($\text{Me}_2\text{-pdt}$) leads to the formation of a clearly semibridging CO group (closest nonbonding $\text{Fe}\cdots\text{C}$ distance 2.78 Å). Both the semibridging and all-terminal CO coordination modes have a predominantly metal–metal bond character in the HOMOs (Figure 5). The relative gas-phase energy of the HOMO in the dimethyl bridgehead (semibridged) complex is higher than that of the monomethyl bridgehead (all-terminal) analogue by approximately 8 kJ mol^{-1} . This would be consistent with bulky bridgehead groups destabilizing the ground state HOMO, lowering $E_{1/2}$ by ca. 83 mV and diminishing activation energies. Notably the experimental difference in oxidation potentials of the monomethyl and dimethyl complexes is ca. 70 mV, in surprisingly good accord with the ground state energy

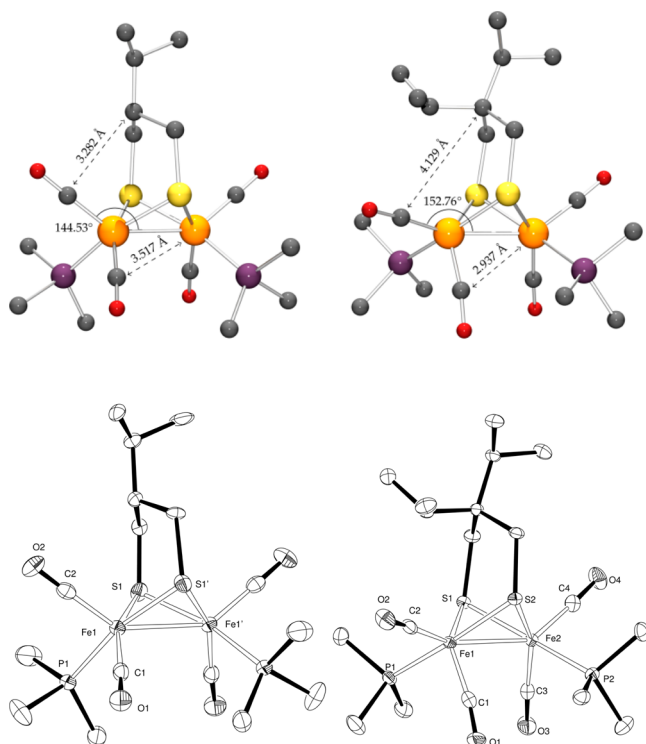


Figure 4. Solid state structures of **1**(*i*Pr-pdt) and **1**(*i*Pr₂-pdt) showing spheres of arbitrary radius (top) and 50% probability ellipsoids (bottom).

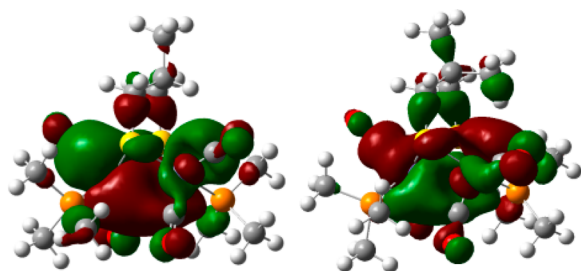


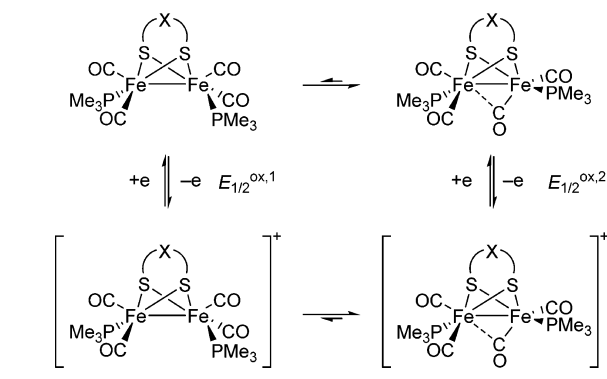
Figure 5. DFT gas-phase HOMO for **1**(Me-pdt) (left) and **1**(Me₂-pdt) (right), showing the two (arbitrary) phases of the orbital in red and green.

difference of ca. 80 mV for the parent complexes as estimated by DFT.

The potential impact of this isomerism on the solution electrochemistry and kinetics can be accommodated by a fast equilibrium between semibridged and terminal isomers as set out in Scheme 2. Although, as clear from the spectroscopic data, the semibridged forms of the dialkyl complexes must be present in low concentrations, a fast pre-equilibrium would shift the redox potential of the dialkyl bridgehead substituted species negative toward that of the more easily oxidized semibridged species, conserving the general correlation between $\ln k_H$, $E_{1/2}^{ox}$ and the energy of the HOMO. Cyclic voltammetry of **1**(Me₂-pdt) in MeCN down to -52°C does not freeze out an equilibrium. There is a negative shift in $E_{1/2}^{ox}$ of ca. 30 mV on cooling from 24 to -52°C , suggesting that the equilibrium must remain fast and shifts toward the semibridging form at lower temperature.

Given in the plot of $(RT/F) \ln k_H$ against $E_{1/2}^{ox}$ (Figure 3, open circles) are data for related systems, **4**–**6**, the two {2Fe3S} complexes and a complex with a benzenedithiolate

Scheme 2. Equilibria between All-Terminal and Semibridging Isomers ($E_{1/2}^{ox,1} > E_{1/2}^{ox,2}$)



bridging unit. While broadly following the trend of the correlation, the complex with the phenylene bridge (**5**) and the thioether complex (**4**) are outliers. In the former case, delocalization of the charge by the noninnocent benzene dithiolate may stabilize the oxidized form accounting for the lower oxidation potential than would be expected from the observed rate. In the case of the thioether complex it might be argued that the SMe group is less polarizable than a PMe₃ substituent, and so is less effective in stabilizing the oxidized form.

Relationship between HOMO Energy and the Basicity of the Metal–Metal Bond. Work by Bordwell and co-workers established linear free energy correlations between pK_a values and the oxidation potential of a series of carbon bases and established for a series of fluorene anions an absolute (dimensionless) Brønsted coefficient close to unity.^{36,37} Moreover, linear free energy correlations have been established between the oxidation potentials and energy of activation of these anions in nucleophilic single electron transfer substitution reactions:³⁸ in this case the Brønsted coefficient was reported to be also close to one. For the series of complexes discussed herein we have similarly established a linear free energy relationship between protonation rate and oxidation potential of the metal–metal bond based HOMO. The magnitude of the Brønsted coefficient for $(RT/F) \ln k_H$ versus $E_{1/2}^{ox}$ is 0.68, and it thus is reasonable to conclude that the activation energy for protonation will correlate to the basicity of the metal–metal bond.²⁹ If we assume that the measured $E_{1/2}$ values for the diiron series are linearly related to the pK_a of the metal–metal bond with a Brønsted coefficient close to unity, $\Delta pK_a/\Delta E_{1/2} = 16.9$ units/V, then the pK_a values of the complexes for which we have directly measured protonation rates span about 9 pK_a units.

The linear free energy relationship derived from the $(RT/F) \ln k_H$ against $E_{1/2}^{ox}$ can be expressed in the general form of eq 1, where β is the Brønsted coefficient and c is a constant that depends on the chosen reference system.

$$\log k_H = \frac{F(c - \beta E_{1/2}^{ox})}{2.303RT} \quad (1)$$

With the estimated value of $\beta = 0.68$ and potentials based relative to the Fc^+/Fc system, $c = 0.012$, the expression can be rearranged using known values for the physical constants at 294 K to that shown in eq 2.

$$\log k_H = 0.20 - 11.7E_{1/2}^{ox} \quad (2)$$

This relationship allows the prediction of the rate of protonation of systems that are not directly amenable to measurement. For example, protonation of 7(pdt) is too fast to measure by SF UV-vis methods ($k_{\text{H}} > 8 \times 10^5 \text{ M}^{-1} \text{ s}^{-1}$), the predicted rate from eq 2 is $1.3 \times 10^{13} \text{ M}^{-1} \text{ s}^{-1}$; bimolecular diffusion-controlled rate constants are typically $<10^9 \text{ M}^{-1} \text{ s}^{-1}$, and it is therefore likely that protonation of this complex is not rate limiting. The complex $\text{Fe}_2(\text{Bn-adt})(\text{CO})_4(\text{PMe}_3)_2$ first protonates at the NBn group,³³ the metal–metal bond is subsequently protonated at a rate retarded by deactivation by the electron-withdrawing bridgehead cationic group NBnH^+ . Using the reported value for $E_{1/2}^{\text{ox}}$ for this complex (-0.26 V vs Fc^+/Fc), eq 2 predicts a rate of direct protonation of the metal–metal bond as ca. $1700 \text{ M}^{-1} \text{ s}^{-1}$, comparable to the other bis(trimethylphosphine) complexes (Table 1). The dicyanide complex $[\text{Fe}_2(\text{pdt})(\text{CO})_4(\text{CN})_2]^{2-}$ similarly protonates kinetically at basic CN^- site rather than the metal–metal bond, subsequently decomposing.³⁹ With the caveat that we are comparing CN^- and PMe_3 substituents, which have different donicities and size, protonation at the metal–metal bond in the dicyanide species may be estimated to have a rate of ca. $8.6 \times 10^5 \text{ M}^{-1} \text{ s}^{-1}$ based on the reported $E_{1/2}^{\text{ox}}$ (-0.49 V vs Fc^+/Fc).⁴⁰ It is interesting to note that Reihner and co-workers have predicted theoretically that protonation of the dicyanide subsite in the enzyme to give a bridging hydride has a high activation energy barrier (39 kcal mol^{-1}) at the Fe(I)Fe(I) level in the enzyme.⁴¹ Although we are very wary of the oversimplification, at an operating potential of -420 mV versus SHE and at pH 7 eq 2 predicts a turnover frequency of ca. 10^3 s^{-1} for the formation of a bridging hydride at the enzyme site, this is an order of magnitude slower than is observed for the enzyme⁴² and consistent with the faster kinetics being associated with protonation to give a terminal hydride.

CONCLUSIONS

The synthesis and characterization of a range of new diiron dithiolate complexes and their bridging hydride derivatives has allowed systematic study of how structure influences protonation at the metal–metal bond. The complexes display second order kinetics on reaction with $\text{HBF}_4 \cdot \text{Et}_2\text{O}$ in MeCN to form the μ -hydrido species. It is found that $\ln k_{\text{H}}$ shows a strong linear correlation with the energy of the HOMO as measured by $E_{1/2}^{\text{ox}}$. The linear free energy relationship allows prediction of rates of protonation where the oxidation potential of the complex is known. Bulky bridgehead substituents are suggested to exert a stereoelectronic influence on the protonation rate. This is explained by the switching of a terminal carbonyl to a semibridging mode, which destabilizes the HOMO, enhancing the protonation rate at the metal–metal bond.

ASSOCIATED CONTENT

Supporting Information

Experimental details for synthesis, stopped-flow and electrochemistry, characterization data, X-ray crystallographic data and DFT details. This material is available free of charge via the Internet at <http://pubs.acs.org>.

AUTHOR INFORMATION

Corresponding Author

c.pickett@uea.ac.uk

Notes

The authors declare no competing financial interest.

ACKNOWLEDGMENTS

We thank the Biotechnology and Biological Sciences Research Council (Grant BB/E023290/1) and Engineering and Physical Sciences Research Council (Grants EP/F047878/1 and EP/H019480/1) for funding. A.J. thanks the University of East Anglia for a studentship. We are grateful to the National Crystallographic Service, University of Southampton and the National Mass Spectrometry Service, Swansea, for data collection. DFT calculations were performed using the High Performance Computing Cluster supported by the Research and Specialist Computing Support Service at the University of East Anglia. We thank Drs. Vasily Oganessian and Richard Stephenson for providing access to Gaussian 09, Dr. S. K. Ibrahim for help with the electrochemical measurements, and James Box and Max Mason-Gransby for the preparation of compounds 1(odt) and 5, respectively.

REFERENCES

- (1) Tard, C.; Pickett, C. J. *Chem. Rev.* **2009**, *109*, 2245–2274.
- (2) (a) Lubitz, W.; Ogata, H.; Rüdiger, O.; Reijerse, E. *Chem. Rev.* **2014**, *114*, 4081–4148. (b) Simmons, T. R.; Berggren, G.; Bacchi, M.; Fontecase, M.; Artero, V. *Coord. Chem. Rev.* **2014**, *270*, 127–150.
- (3) Camara, J. M.; Rauchfuss, T. B. *Nat. Chem.* **2012**, *4*, 26–30.
- (4) Ghosh, S.; Hogarth, G.; Hollingsworth, N.; Holt, K. B.; Kabir, S. E.; Sanchez, B. E. *Chem. Commun.* **2014**, *50*, 945–947.
- (5) Hoffman, B. M.; Lukoyanov, D.; Dean, D. R.; Seefeldt, L. C. *Acc. Chem. Res.* **2013**, *46*, 587–595.
- (6) Lindahl, P. A. *Biochemistry* **2002**, *41*, 2097–2105.
- (7) For an early biomimetic example, see: Zhao, X.; Georgakaki, I. P.; Miller, M. L.; Yarbrough, J. C.; Darensbourg, M. Y. *J. Am. Chem. Soc.* **2001**, *123*, 9710–9711.
- (8) Ezzaher, S.; Capon, J.-F.; Gloaguen, F.; Pétillon, F. Y.; Schollhammer, P.; Talarmin, J. *Inorg. Chem.* **2007**, *46*, 3426–3428.
- (9) Barton, B. E.; Rauchfuss, T. B. *Inorg. Chem.* **2008**, *47*, 2261–2263.
- (10) Zaffaroni, R.; Rauchfuss, T. B.; Gray, D. L.; De Gioia, L.; Zampella, G. *J. Am. Chem. Soc.* **2012**, *134*, 19260–19269.
- (11) Wang, W.; Rauchfuss, T. B.; Zhu, L.; Zampella, G. *J. Am. Chem. Soc.* **2014**, *136*, 5773–5782.
- (12) van der Vlugt, J. I.; Rauchfuss, T. B.; Wilson, S. R. *Chem.—Eur. J.* **2005**, *12*, 90–98.
- (13) Wright, J. A.; Pickett, C. J. *Chem. Commun.* **2009**, *45*, 5719–5721.
- (14) Jablonskytė, A.; Wright, J. A.; Pickett, C. J. *Dalton Trans.* **2010**, *39*, 3026–3034.
- (15) Jablonskytė, A.; Wright, J. A.; Pickett, C. J. *Eur. J. Inorg. Chem.* **2011**, 1033–1037.
- (16) Singleton, M. L.; Bhuvanesh, N.; Reibenspies, J. H.; Darensbourg, M. Y. *Angew. Chem., Int. Ed.* **2008**, *47*, 9492–9495.
- (17) Kramarz, K. W.; Norton, J. R. *Prog. Inorg. Chem.* **1994**, *42*, 1–65.
- (18) Henderson, R. A.; Oglieve, K. E. *J. Chem. Soc., Dalton Trans.* **1993**, *22*, 3431–3439.
- (19) Henderson, R. A.; Ibrahim, S. K.; Oglieve, K. E.; Pickett, C. J. *J. Chem. Soc., Chem. Commun.* **1995**, *31*, 1571–1572.
- (20) Grönberg, K. L. C.; Henderson, R. A.; Oglieve, K. E. *J. Chem. Soc., Dalton Trans.* **1998**, *27*, 3093–3104.
- (21) Singleton, M. L.; Jenkins, R. M.; Klemashevich, C. L.; Darensbourg, M. Y. *C. R. Chim.* **2008**, *11*, 861–874.
- (22) Hsieh, C.-H.; Erdem, Ö. F.; Harman, S. D.; Singleton, M. L.; Reijerse, E.; Lubitz, W.; Popescu, C. V.; Reibenspies, J. H.; Brothers, S. M.; Hall, M. B.; Darensbourg, M. Y. *J. Am. Chem. Soc.* **2012**, *134*, 13089–13102.
- (23) Zhao, X.; Georgakaki, I. P.; Miller, M. L.; Mejia-Rodriguez, R.; Chiang, C.-Y.; Darensbourg, M. Y. *Inorg. Chem.* **2002**, *41*, 3917–3928.
- (24) Protonation of 2(pdt) has been reported under superacidic conditions: Matthews, S. L.; Heinekey, D. M. *Inorg. Chem.* **2010**, *49*, 9746–9748.

- (25) Teo, B. K.; Hall, M. B.; Fenske, R. F.; Dahl, L. F. *Inorg. Chem.* **1975**, *14*, 3103–3117.
- (26) Andersen, E. L.; Fehlner, T. P.; Foti, A. E.; Salahub, D. R. *J. Am. Chem. Soc.* **1980**, *102*, 7422–7429.
- (27) Walther, B.; Hartung, H.; Reinhold, J.; Jones, P. G.; Mealli, C.; Bottcher, H. C.; Baumeister, U.; Krug, A.; Mockelt, A. *Organometallics* **1992**, *11*, 1542–1549.
- (28) Bard, A. J.; Faulkner, L. R. *Electrochemical Methods: Fundamentals and Applications*, 2nd Ed.; John Wiley & Sons: Chichester, U.K., 2001.
- (29) Sarapu, A. C.; Fenske, R. F. *Inorg. Chem.* **1975**, *14*, 247–253.
- (30) Pickett, C. J.; Pletcher, D. J. *Organomet. Chem.* **1975**, *102*, 327–333.
- (31) For reversible systems $E_{1/2}$ is independent of temperature if, as is usually the case, the ratio of the diffusion coefficient for the oxidized and reduced partners is closely similar at all temperatures. Whether the slope, viz. $\Delta\Delta G^\ddagger/\Delta E_{1/2}$, varies with T will essentially depend on whether changes in the entropy of activation $\Delta\Delta S^\ddagger$ varies significantly across the series. The observed correlation indicates the entropic contribution to ΔG^\ddagger associated with the ordering of the transition state is similar for all of the complexes or varies monotonically with ΔH^\ddagger . In either case $\Delta\Delta S^\ddagger$ is probably small, and consequently the effect of T on the slope is likely to be small with $\Delta\Delta G^\ddagger$ and dominated by the enthalpic $\Delta\Delta H^\ddagger$ terms.
- (32) Chatt, J.; Leigh, G. J.; Neukomm, H.; Pickett, C. J.; Stanley, D. R. *J. Chem. Soc., Dalton Trans.* **1980**, 121–127.
- (33) Eilers, G.; Schwartz, L.; Stein, M.; Zampella, G.; de Gioia, L.; Ott, S.; Lomoth, R. *Chem.—Eur. J.* **2007**, *13*, 7075–7084.
- (34) A further factor that we have considered that might trend with protonation rates is variation in metal–metal bond distances in the reactants and products. There is not a systematic dependence on reactant or product bond lengths, or changes of these (Table S1, SI).
- (35) “Rotated” states at the Fe(I)Fe(I) level have been generated by the introduction of steric bulk at the bridgehead (ref 22) and by combining steric bulk with electronic asymmetry: Sabrina; Munery; Capon, J.-F.; De Gioia, L.; Elleouet, C.; Greco, C.; Pétillon, F. Y.; Schollhammer, P.; Zampella, G. C. *Chem.—Eur. J.* **2013**, *19*, 15458–15461. Wang, W.; Rauchfuss, T. B.; Moore, C. E.; Rheingold, A. L.; De Gioia, L.; Zampella, G. *Chem.—Eur. J.* **2013**, *19*, 15476–15479. De Gioia, L.; Elleouet, C.; Munery, S.; Pétillon, F. Y.; Schollhammer, P.; Talarmin, J.; Zampella, G. *Eur. J. Inorg. Chem.* **2013**, 3456–3461. The latter exhibit fully rotated states and bridging carbonyl groups, while the former are best viewed as partially “twisted”. In the natural system, the geometry at the metal center is fully rotated with a bridging CO present, although the influence of the enzyme scaffold is also likely responsible for maintaining the rotated state.
- (36) Bordwell, F. G.; Bausch, M. J. *J. Am. Chem. Soc.* **1986**, *108*, 1979–1985.
- (37) Bordwell, F. G.; Bausch, M. J. *J. Am. Chem. Soc.* **1986**, *108*, 1985–1988.
- (38) Angelici, R. J. *Acc. Chem. Res.* **1995**, *28*, 51–60.
- (39) Wright, J. A.; Webster, L.; Jablonskytė, A.; Woi, P. M.; Ibrahim, S. K.; Pickett, C. J. *Faraday Discuss.* **2011**, *148*, 359–371.
- (40) Le Cloirec, A.; Best, S. P.; Borg, S.; Davies, S. C.; Evans, D. J.; Hughes, D. L.; Pickett, C. J. *Chem. Commun.* **1999**, 35, 2285–2286.
- (41) Finkelmann, A. R.; Stiebritz, M. T.; Reiher, M. *Chem. Sci.* **2014**, *5*, 215–221.
- (42) Frey, M. *ChemBioChem* **2002**, *3*, 153–160.